



X. R. Liu · Q. Sun

An improved macro–micro-two-scale model to predict high-cycle fatigue life under variable amplitude loading

Received: 17 June 2020 / Accepted: 26 November 2020 / Published online: 1 January 2021
© The Author(s), under exclusive licence to Springer-Verlag GmbH, DE part of Springer Nature 2021

Abstract This study is based on continuum damage mechanics and constructs an improved macro–micro-two-scale model to predict the fatigue life of engineering metallic materials subjected to variable amplitude loading. To account quantitatively for the fatigue damage retarding effect of higher load on lower ones in a loading sequence, the cyclic plastic response curve of microscopic weak inclusion is independently designed. Meanwhile, an improved two-scale fatigue damage model in rate form is proposed by introducing a new exponent function acted on the equivalent plastic strain term in the model for taking account of fatigue mean stress effect under variable amplitude loading. The parameters of the two-scale fatigue damage model are identified through an inverse approach based on fatigue test results under constant amplitude loading. The predictive accuracy of the proposed model is validated by fatigue test data of Al 2024-T3 standard coupon and plate with a hole under different variable amplitude loading.

Keywords Continuum damage mechanics · Metallic materials · Fatigue life · Retarding effect · Two-scale model

1 Introduction

Metallic materials remain a dominate proportion in engineering structure, especially for key load transmission parts. Fatigue damage caused by cyclic loading in long-term working period is one of the main failure modes of metal components, which is always the focus of safety and reliability prediction [1]. In the prediction of engineering fatigue failure, metal components are macroscopically considered as continuum. In fact, the fatigue damage or crack initiation and growth always originate from large numbers of microscopic dislocation movement and defects evolution [2, 3]. S–N curves and Palmgren–Miner linear damage accumulation principle are still valid methods [4], but often give unduly conservative prediction results for a variable amplitude or random loading sequence applied to an engineering component [5]. The main reason leading to poor prediction is the so-called retard effect of foregoing higher amplitude loads on subsequent lower ones in a fatigue loading sequence. The retardation results from the local residual compressive stress effect caused by unloading of

Communicated by Andreas Öchsner.

X. R. Liu
School of Aeronautical Engineering, Zhengzhou University of Aeronautics, Zhengzhou 450046, China

X. R. Liu
Research Institute of Unmanned Aerial Vehicles, Zhengzhou University of Aeronautics, Zhengzhou 450046, China

Q. Sun (✉)
School of Aeronautics, Northwestern Polytechnical University, Xi'an 710072, China
E-mail: sunqin@nwpu.edu.cn

those higher amplitude loads. The key point to estimate fatigue damage accumulation in a variable amplitude loading spectrum is to quantify the localized residual compressive stress effect and the influence on evolution of microstructural defects, the study of which still remains open up to date [6].

A way to avoid a micromechanical analysis for each type of defect and mechanism of damage is to postulate a principle at the mesoscale [7]. From the perspective of mesoscale mechanics, a model to quantify the microstructural damage evolution can be created by means of a weak inclusion surrounded by infinite homogenous medium, since the damage evolution always deteriorates or weakens the mechanical behavior of an engineering component. The theoretical inclusion model is also known as macro–micro–two-scale model. The macro–micro–two-scale model has developed in the past several decades. Eshelby [8] studied macro–micro-connecting factor of ellipsoid inclusion. Hill [9,10] and Iwakuma [11] focused on the transmission of quantities from macroscale to microscale. [12,13] provides an effective pathway to evaluate microscopic stress and strain of weak inclusions by means of a set of the derived bridging equations. Pierard [14] studied plastic theory of ellipsoid inclusion at the microscale.

The two-scale concept has been extended further to study fatigue damage accumulation and predict fatigue life for high cycles [7,15,16]. Lemaitre et al. [17,18] established a high-cycle fatigue evolution model based on the stress–strain state of microscopic weak inclusion. The model can reflect the effect of mean stress and nonlinear damage accumulation. Many researchers predicted the fatigue life of various materials with macro–micro–two-scale damage model [19–22]. However, there still exist some issues or simplifications in the most of above-mentioned works. The assumed plastic stress–strain curve for a microscale weak inclusion is fully similar to macroscale matrix. The only difference comes from the length of linear elastic segment, which causes another trouble to determine the yield stress for microscale, and leads to incorrect microscopic hysteresis loop response to different amplitude loadings at macroscale. The above-mentioned issues cause retardation effect cannot be adequately quantified in two-scale model. So it is necessary to improve microscopic hysteresis loop response to macroscale loadings so that the fatigue damage accumulation under variable amplitude or random spectrum loading can be estimated reasonably.

In this paper, from the engineering point of view, the hysteresis loop curve accounting for nonlinear plastic hardening for weak inclusion is independently designed to effectively estimate retarding effect. The Lemaitre's fatigue damage evolution model is modified by introducing a new exponent to take account of mean stress effect. Fatigue tests of Al-alloy under multi-level constant amplitude loading, especially for high-cycle fatigue, have been performed to identify the model parameters. The new macro–micro–two-scale fatigue damage evolution model in this study is coded as post-processor, and the effectiveness of which is verified through fatigue tests under variable amplitude loading and random loading.

2 Elastoplastic stress–strain curve with hysteresis loop at microscale

In the two-scale model for high-cycle fatigue damage prediction, both to determine the stress–strain curve with plastic hardening law for weak inclusion and to calculate the microscopic stress–strain field in a critical spot of engineering structure are two imperative procedures. This section will be devoted to construct the whole elastoplastic stress–strain curve for the improvement of microscopic hysteresis loop response to any variable loading spectrum applied to an engineering component.

2.1 A brief overview of two-scale model solution procedure

The analytical solution to stress–strain of an infinitesimal inclusion built into infinite elastoplastic body dates from middle of twentieth century. The macro–micro-bridging equations [18,23], which combine Eshelby-Kroner's localization law with elasto-plastic constitutive equations, can be expressed as

$$\begin{cases} \boldsymbol{\varepsilon}^\mu = \boldsymbol{\varepsilon} + \beta(\boldsymbol{\varepsilon}^{\mu P} - \boldsymbol{\varepsilon}^P) \\ \boldsymbol{\sigma}^\mu = \mathbf{D}^e \boldsymbol{\varepsilon}^{\mu e} = \boldsymbol{\sigma} - a\mathbf{D}^e (\boldsymbol{\varepsilon}^{\mu P} - \boldsymbol{\varepsilon}^P) \\ f^\mu = (\boldsymbol{\sigma}^\mu - \mathbf{X}^\mu)_{eq} - \sigma_y^\mu = 0 \\ \mathbf{X}^\mu = C_y^\mu \boldsymbol{\varepsilon}^{\mu P} \\ \sigma_y^\mu = \sigma_{y0}^\mu + R^\mu = \sigma_{y0}^\mu + H^\mu \varepsilon_{eq}^{\mu P} \end{cases} \quad (1)$$

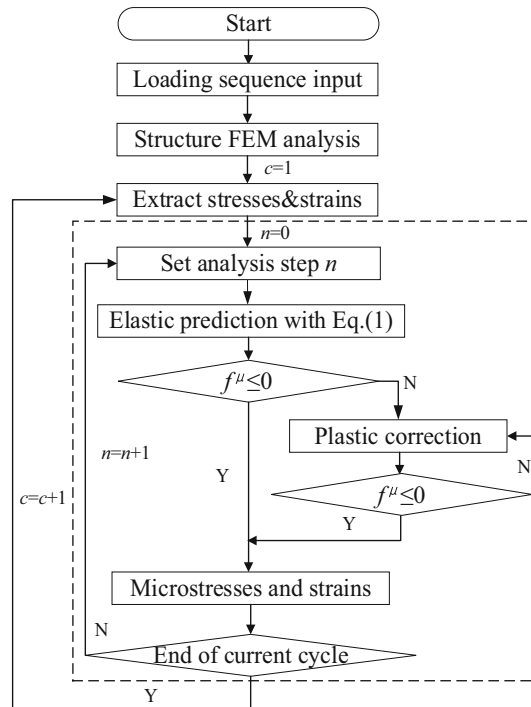


Fig. 1 Flowchart of solution procedure

where a and β are given by the Eshelby's closed solution of a spherical inclusion:

$$a = \frac{1 - \beta}{1 + \nu}, \quad \beta = \frac{2(4 - 5\nu)}{15(1 - \nu)} \quad (2)$$

where ν is Poisson's ratio.

In Eq. (1), the superscript μ means microscale; σ^μ , $\epsilon^{\mu e}$ and $\epsilon^{\mu p}$ are the unknown stresses, elastic and plastic strains of the inclusion; f^μ is the yield function; \mathbf{X}^μ is the kinematic hardening back stress; R^μ is the incremental size of the yield surface because of isotropic hardening; C_y^μ and H^μ are the plastic tangent moduli of kinematic and isotropic hardening quantities, respectively; \mathbf{D}^e is the elastic modulus which is always identical for the two scales; σ , ϵ and ϵ^p indicate the known uniform stresses, total and plastic strains at macroscale, respectively.

The stresses and strains at the critical spot of a structure can be calculated by conventional finite element analysis. The variable peak-valley values in a loading sequence are original inputs for the post-processing calculation of microscopical stresses and strains. Due to nonlinear plasticity at microscale, an implicit increment integration process must be implemented, which includes the two major iterative procedures of elastic prediction and plastic correction. The algorithmic flowchart of integration solution is illustrated in Fig. 1.

2.2 Stress–strain constitutive curve at microscale

As mentioned above, the plastic stress–strain curve at microscale in currently published works was assumed to be the same as that at macroscale. The yield stress of the microscopic inclusion is taken as macroscopic engineering fatigue strength σ_{-1} . The macroscopic engineering fatigue strength is a conditioned value and varies as the function of stress ratio. Thus, the microscopic elastoplastic curve is not unique. Meanwhile, the same plastic stress–strain curve for two scale will lead to an unreasonable microscopic stress–strain response to macroscopically variable amplitude loadings. Take Al 2024-T3 as example, fatigue strength σ_{-1} is approximate 90 MPa at 10^7 cycles, which is taken as the yield stress of microscopic inclusion according to traditional methods. When the macroscopic loading is an asymmetric constant-amplitude load sequence with $R = 0.06$ and $S_{\max} = 200$ MPa, the microscale hysteresis loops are calculated and illustrated in Fig. 2. It can be seen that the subsequent microscale hysteresis loops disappear after the first cyclic loading. It means theoretically

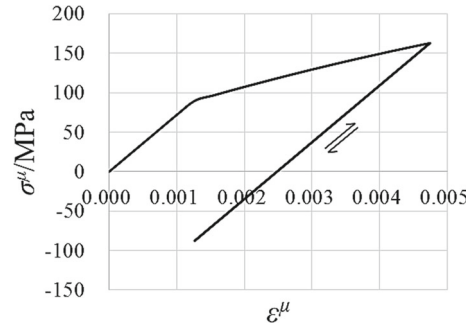


Fig. 2 Microscopic stress–strain hysteresis curves under macroscopically asymmetric elastic loadings

that no fatigue damage at microscale will occur after the first cycle, which is not consistent with fact. It is because the microscopic yield stress and plastic hardening parameters are not reasonable.

In fact, it is rational to assume stress–strain curve for two scale to be different in view of specifically microscopic plastic physics and for the purpose to use two-scale model for fatigue damage prediction. To avoid microscale analysis, the mechanical properties of microscale weak inclusion should be designed independently in accordance with possible requirement to macro–micro–two-scale model. It means that the microscopic kinematic and isotropic hardening properties different from macroscopic ones need to be built for taking account of the influence of higher loads on subsequent lower ones.

For most metallic materials in engineering, the uniaxial plastic stress–strain curve can be expressed as an exponential function [24],

$$\sigma^\mu = \sigma_0^\mu + Q_\infty^\mu (1 - e^{-b\bar{\varepsilon}_p^\mu}) \quad (3)$$

where σ_0^μ is initial yield stress, Q_∞^μ is plastic hardening increment from initial yield to failure stress, b is model coefficient and $\bar{\varepsilon}_p^\mu$ is equivalent plastic strain.

Most metallic materials in engineering show both kinematic and isotropic hardening behaviors after initial yield. For the simplicity to determine the relationship between kinematic and isotropic hardening laws at microscale, a proportional hardening model [25] is chosen in this paper. The isotropic hardening term can be taken as

$$R^\mu = M Q_\infty^\mu (1 - e^{-b\bar{\varepsilon}_p^\mu}) \quad (4)$$

and then kinematic hardening term is written as

$$X^\mu = (1 - M) Q_\infty^\mu (1 - e^{-b\bar{\varepsilon}_p^\mu}) \quad (5)$$

The key point to use the proportional hardening model for microscale is to define properly the yield stress σ_0^μ , the constants Q_∞^μ and b as well as the proportional parameter M .

2.3 Parameters selection for macro–micro–two-scale model

To attain more accurate prediction of high-cycle fatigue damage accumulation in a variable amplitude loading sequence with two-scale model, two basic principles can be established to avoid the foregoing deficiencies. First, from more conservative point of view, any stress lower than the engineering fatigue strength under different stress ratios can be chosen as yield stress at microscale so that microscopic stresses can easily go beyond its yielding point under small stress amplitude loading. Second, a stabilized hysteresis loop at microscale should be obtained under different stress ratio cyclic loading with relative small stress amplitudes at macroscale.

Based on the above principles, plastic parameters at microscale should be set to ensure there are stabilized plastic hysteresis loops under variable amplitude loading. Therefore, the quantity Q_∞^μ in Eq. (3) can be relatively moderate; the exponent factor b should be chosen reasonably to speed up the stabilization of hysteresis loop; and the proportional parameter M in Eq. (4) cannot be greater than 0.5 to keep hysteresis loop response at microscale as soon as possible. Thus, plastic parameters at microscale for Al 2024-T3 are set as follows. The initial yield stress σ_{y0}^μ is set to 20 MPa, Q_∞^μ to 70 MPa, b to 200 MPa and M to 0.45. Using the designed

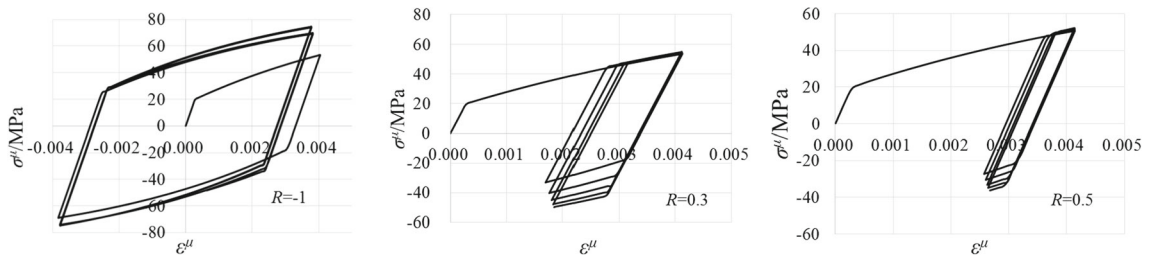


Fig. 3 Comparisons of hysteresis loops under different stress ratio loading

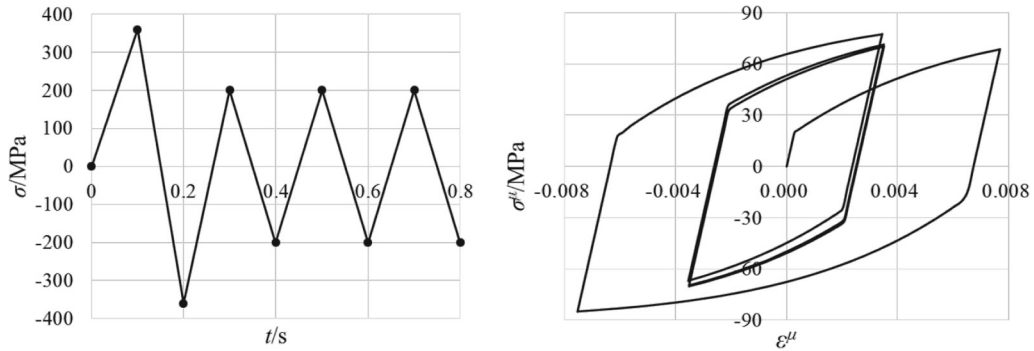


Fig. 4 Microscopic elastoplastic hysteresis loops under variable amplitude loading

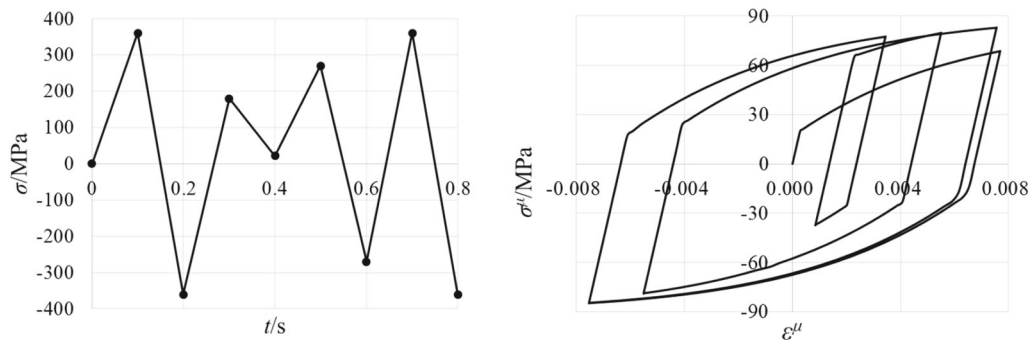


Fig. 5 Microscopic elastoplastic hysteresis loops under random loading

parameters, the following numerical examples are completed under different stress ratio cyclic loading with same maximum stress, 200 MPa within the macroscopic elasticity. The resulting hysteresis loops at microscale are illustrated in Fig. 3. It can be seen that stabilized hysteresis loop still can be reached even when $R = 0.3$.

To show the variation of microscopic hysteresis loops influenced due to higher load, a variable amplitude cyclic loading example under macroscale elastic condition is illustrated in Fig. 4. The stress amplitude of first cyclic loading is 360 MPa, the subsequent stress amplitudes are 200 MPa, and all the stress ratio $R = -1$. The resulting microscopic plastic strain range of subsequent stabilized hysteresis loop is 0.559% in this case as illustrated in Fig. 4. Compared with the first case of constant amplitude loadings in the left side of Fig. 3, the corresponding plastic strain range is 0.617%, which just reveals that less fatigue damage is accumulated after higher load. Another example under random loadings is shown in Fig. 5.

3 Fatigue damage model and the parameters identification

Once the stress–strain field at microscale is obtained as shown in section 2, the fatigue damage evolution under elastic variable amplitude loading can be quantified in a more accurate way. In terms of two-scale fatigue damage predictive model, the fatigue damage can be evaluated by the sizes of microscopic hysteresis loops, which is similar to macroscopic low-cycle fatigue prediction. So the fatigue damage evolution model

at microscale and its parameters should be identified firstly. Moreover, the mean stress effect also needs to be taken into account for a variable amplitude or random spectrum loading.

3.1 Fatigue damage evolution model

A better fatigue damage evolution equation for microscale has been proposed through long-term research works by Lemaitre et al. [18]. Lemaitre introduced the crack closure parameter h in the fatigue damage evolution model to obtain the influence of the mean stress. However, in the case of tension–tension loading, the model cannot account for influence of mean stress.

Thus, the present study proposes modified version of Lemaitre’s model, which can obtain influence of mean stress even in case of tension–tension variable amplitude loadings. The model is written as

$$\begin{aligned} \dot{D} &= \left(\frac{Y^\mu}{S} \right)^s (\dot{p}^\mu)^q \\ \int_t \dot{D} dt &= D_c \end{aligned} \quad (6)$$

where \dot{D} is fatigue damage evolution rate; \dot{p}^μ is equivalent plastic strain rate at microscale; D_c is the threshold value of fatigue failure at microscale; the quantity Y^μ originally denotes the strain energy density release rate when microscopic fatigue damage occurs progressively and can be derived for multiaxial stress state from unloading modulus variation,

$$Y^\mu = \frac{\sigma_{eq}^{\mu 2}}{2E(1-D)^2} R_v^\mu, \quad R_v^\mu = \left[\frac{2}{3}(1+\nu) + 3(1-2\nu) \left(\frac{\sigma_m^\mu}{\sigma_{eq}^\mu} \right)^2 \right] \quad (7)$$

where σ_{eq}^μ is von Mises equivalent stress, σ_m^μ is spherical stress, E is Young’s modulus, ν is Poisson’s ratio, and R_v^μ is triaxiality function, which is used to account for the influence of hydrostatic stress or triaxiality ratio.

In Eq. (6), a controversial issue is how to understand and use the quantity Y^μ clearly at microscale. Because the unloading modulus is not sensitive to fatigue damage before the damage goes up to macroscale threshold. In this case, we would rather understand Y^μ as elastic potential energy stored in the metallic microstructure in every complete hysteresis loop from micro-physical perspective. In order to match the released elastic potential energy when fatigue damage occurs at microscale, the parameter S in Eq. (6) is used to scale down the nominal quantity Y^μ and another exponent term s is used for its nonlinear effect on fatigue damage.

For a variable amplitude or random loading spectrum, another important contributor to fatigue damage arises from variable mean stress, which is referred as fatigue creep or ratcheting effect. A new exponent term q is introduced into Eq. (6) to accommodate the nonlinear effect of the equivalent plastic strain rate \dot{p}^μ on fatigue damage, which is written as a function of stress amplitude,

$$q = B \lg S_a + A \quad (8)$$

where S_a is stress amplitude under $R = -1$. It is transformed from arbitrary loading with different mean stress and stress amplitude according to Goodman constant life diagram [26], which is written as Eq. (3). So q is not only a function of stress amplitude, it also takes account of mean stress effect.

$$S_a = \frac{S_{a0} \cdot \sigma_0}{\sigma_0 + \left(\frac{1+R}{1-R} - \frac{1+R_0}{1-R_0} \right) S_{a0}} \quad (9)$$

where σ is ultimate strength, S_a and R are the stress amplitude and stress ratio of practical loading.

For high-cycle fatigue, the damage model at microscale to calculate the accumulated damage in half a cycle is written in detail as,

$$\frac{dD}{dN_{half}} = \begin{cases} \left(\frac{R_v^\mu \sigma_{eq,\max}^{\mu 2}}{2ES(1-D)^2} \right)^s (p^\mu)^q, & \varepsilon_{\min}^\mu \geq 0 \\ 0.2 \times \left(\frac{R_v^\mu \sigma_{eq,\max}^{\mu 2}}{2ES(1-D)^2} \right)^s (p^\mu)^q, & \varepsilon_{\min}^\mu < 0 \text{ and } \varepsilon_{\max}^\mu > 0 \end{cases} \quad (10)$$

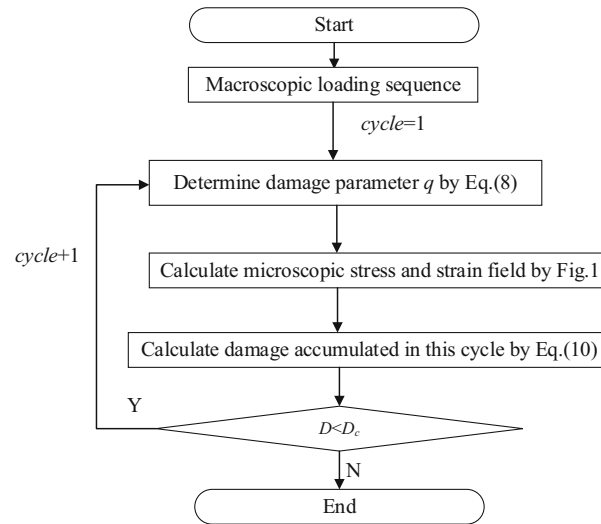


Fig. 6 Fatigue life prediction procedure of two-scale model

The crack closure effect is taken into account by introducing a coefficient for compression which is always 0.2 for metal. The superscript μ means the quantities at microscale. ε_{\min}^{μ} and ε_{\max}^{μ} are minimum and maximum of maximum principal strain, respectively, which are used to determine whether stress state is tension or compression.

Once parameters S , s and q are achieved. Macroscopic stress and strain fields at critical spot of component under loading sequence are calculated by FEM analysis. Microscopic stress and strain fields can be solved by Fig. 1. Fatigue life can be calculated by substituting S , s and q into the microscopic damage evolution model. Fatigue life prediction procedure is illustrated in Fig. 6.

3.2 Identification of model parameters

S , s and q in Eq. (6) should be identified in advance. When stress level and the other parameters are determined, fatigue life can be seen as a function of S , s and q , which is written as

$$N = f(S, s, q) \quad (11)$$

In general, model parameters can be identified through an inverse approach. In the least squares sense, an objective function representing difference between experimental and predicted lives has been built and minimized using SQP algorithm [27]. The optimization procedure is written as,

$$F(S, s, q) = \min \frac{\sum_{k=1}^a [(f_k(S, s, q) - N_{fk})^2]}{\sum_{k=1}^a N_{fk}^2} \quad (12)$$

$$s.t. \quad \begin{aligned} 0 &\leq s \leq 5 \\ 0 &\leq S \leq 5 \\ 0 &\leq q \leq 5 \end{aligned}$$

where a is number of fatigue test data, N_{fk} is fatigue test lives under different stress levels. It should be noticed that the inverse identification is robust since the determined damage parameters are insensitive to the initial values. Indeed, using two different initial values, the algorithm converges to identical identified results which are the global minimum values.

Fatigue test of aluminum alloy 2024-T3 coupons has been performed under 6 different constant amplitude stress levels and stress ratio $R = -1$. Test machine is Instron 8802. Test is conducted according to ASTM E466-15, i.e., standard practice for conducting force controlled constant amplitude axial fatigue tests of metallic materials. The configuration of tested specimen is illustrated in Fig. 7. All dimensions are in millimeters (mm). Controlled parameter is force. Loading frequency is 10 Hz. Stress amplitude range should be less than yield

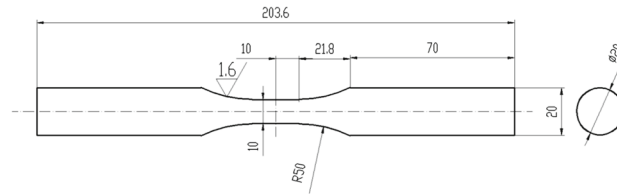


Fig. 7 Configuration of tested coupons



Fig. 8 Specimens for fatigue test

Table 1 Fatigue test results under constant amplitude loading

| Stress amplitude/MPa | Test life | Mean value |
|----------------------|--|------------|
| 360 | 5503, 7355, 7983, 6016 | 6714 |
| 315 | 14,542, 19,515, 12,181, 17,905, 14,202 | 15,669 |
| 270 | 36,770, 39,729, 32,528, 53,710, 26,296 | 37,807 |
| 225 | 1,03,802, 1,59,956, 1,49,417, 1,13,396, 1,88,604 | 1,43,035 |
| 200 | 7,75,796, 4,21,346, 1,90,824, 2,53,911, 3,89,915 | 4,06,358 |
| 180 | 2,004,958, 7,24,338, 9,05,673, 3,512,550 | 1,786,880 |

Table 2 Fitted results of S , s and q

| Stress amplitude/MPa | 360 | 315 | 270 | 225 | 200 | 180 |
|----------------------|--------|--------|--------|--------|--------|--------|
| S | 3.6782 | 3.6714 | 3.6750 | 3.6679 | 3.6755 | 3.6916 |
| s | 1.5638 | 1.5708 | 1.5748 | 1.5678 | 1.5754 | 1.5810 |
| q | 0.7066 | 0.8391 | 0.9499 | 1.1607 | 1.3002 | 1.5132 |

stress. End of fatigue test criterion is complete separation. Some specimen samples are shown in Fig. 8. Test results are listed in Table 1.

Eventually, the fitting S , s and q under 6 stress levels are obtained and listed in Table 2. It can be seen that S and s almost keep unchanged under 6 stress levels. So S and s can be regarded as material constant. The mean value of S and s under 6 stress levels is 3.6766 and 1.5723, respectively. Meanwhile, q changes with stress amplitude. Fitted results of Eq. (2) are listed in Table 3, where R is linear correlation coefficient.

Table 3 Fitted results of coefficient B and A

| B | A | R |
|---------|--------|---------|
| -2.5621 | 7.2250 | -0.9890 |

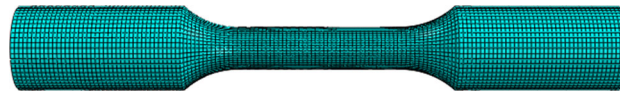


Fig. 9 Finite element model of specimen

4 Verification of the proposed model and discussions

The macro–micro-two-scale model along with fatigue damage evolution model is coded as a post-processor to calculate accumulated damage in every cycle. When accumulated damage D reaches threshold D_c , the number of cycles is fatigue life. The implementation of proposed model can be divided into two stages. First, obtain peak-valley value of macroscopic stresses and strains at critical spot for every cycle through finite element analysis. Especially for high cycle, if the loading is proportional, only one elastic FE computation under reference loading is needed. Then peak-valley value of stresses and strains for every cycle can be computed directly through the proportion to reference loading. Second, the obtained quantities in first stage are the input of post-processor. Then the fatigue life can be estimated.

4.1 Verification under constant amplitude loading

The finite element model of specimen is established in ABAQUS as Fig. 9. The element type is C3D8R, which is three-dimensional, 8-node linear brick, reduced integration and hourglass control element.

Under the 6 stress levels, the fatigue life is predicted by proposed model. The comparisons between predicted fatigue lives and test lives are listed in Table 4.

It can be seen that the maximum error is 14.85%, which is acceptable in engineering. However, results are obtained only under stress ratio $R = -1$. Tests under different stress ratio are needed to validate applicability of the macro–micro-two-scale fatigue damage model.

Tests under two stress levels when stress ratio $R = 0.06$ were performed. Results are listed in Table 5.

Similarly, comparisons between predicted fatigue life and test life under $R = 0.06$ are listed in Table 6. It should be noted that stress amplitude S_a under $R = 0.06$ should be converted through Eq. (3).

It can be concluded that the maximum error under $R = 0.06$ is -19.02% . The macro–micro-two-scale damage model can predict fatigue life properly under constant amplitude loading under different stress ratio.

Table 4 Comparisons between predicted lives and test lives under constant amplitude loading

| Stress amplitude/MPa | 360 | 315 | 270 | 225 | 200 | 180 |
|----------------------|------------|-----------|-----------|----------|-----------|------------|
| Test mean life | 6714 | 15,669 | 37,807 | 1,43,035 | 4,06,358 | 1,786,880 |
| Predicted life | 6022 | 14,758 | 42,740 | 1,49,578 | 4,66,720 | 1,594,000 |
| Error | -10.31% | -5.81% | 13.05% | 4.57% | 14.85% | -10.79% |

Table 5 Fatigue test results under $R = 0.06$

| Stress amplitude/MPa | Test life | Mean value |
|----------------------|------------------------|------------|
| 200 | 19,333, 36,277, 29,700 | 28437 |
| 180 | 69,652, 94,344, 62,589 | 75528 |

Table 6 Comparisons between predicted life and test life under $R = 0.06$

| Stress amplitude/MPa | Test mean life | Predicted life | Error |
|----------------------|----------------|----------------|------------|
| 200 | 28,437 | 23,029 | -19.02% |
| 180 | 75,528 | 62,381 | -17.41% |

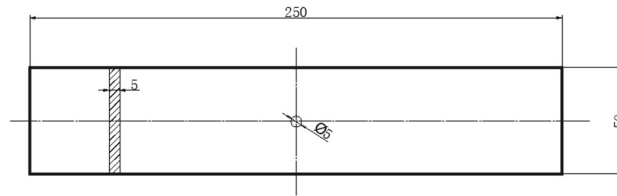


Fig. 10 Configuration of tested specimen

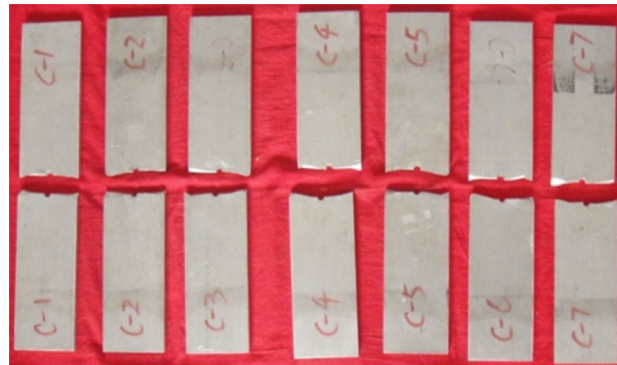


Fig. 11 The fractured specimens

Table 7 Stress and number of cycles for each level in group B1

| Level | S_{\max} (MPa) | R | Number of cycles | f (Hz) |
|-------|------------------|------|------------------|----------|
| 1 | 71.0 | 0.06 | 600 | 10 |
| 2 | 53.4 | 0.06 | To failure | 18 |

Table 8 Stress and number of cycles for each level in group B2

| Level | S_{\max} (MPa) | R | Number of cycles | f (Hz) |
|-------|------------------|------|------------------|----------|
| 1 | 53.4 | 0.06 | 3500 | 20 |
| 2 | 130.0 | 0.06 | 100 | 5 |
| 3 | 53.4 | 0.06 | 3500 | 20 |

4.2 Verification under blocked and random spectrum loading

Most complex components are subjected to blocked or random spectrum loading in engineering. To validate the more general applicability of the two-scale damage model, fatigue tests of aluminum alloy 2024-T3 plate with hole under 7 groups of blocked spectrum loading and 1 group of random spectrum loading have been performed. The configuration of tested specimen is illustrated in Fig. 10. All dimensions are in millimeters (mm). Some fractured specimen samples are illustrated in Fig. 11.

The maximum stress, minimum stress and number of loading cycles for each level in 7 groups of blocked spectrum loading are listed in Tables 7, 8, 9, 10, 11, 12 and 13. The test results of blocked spectrum loading are listed in Table 14.

Table 9 Stress and number of cycles for each level in group B3

| Level | S_{\max} (MPa) | R | Number of cycles | f (Hz) |
|-------|------------------|------|------------------|----------|
| 1 | 53.4 | 0.06 | 500 | 20 |
| 2 | 130.0 | 0.06 | 10 | 5 |
| 3 | 53.4 | 0.06 | 500 | 20 |

Table 10 Stress and number of cycles for each level in group B4

| Level | S_{\max} (MPa) | R | Number of cycles | f (Hz) |
|-------|------------------|------|------------------|----------|
| 1 | 40.0 | 0.06 | 10,000 | 20 |
| 2 | 53.4 | 0.06 | 1600 | 18 |
| 3 | 130.0 | 0.06 | 100 | 5 |
| 4 | 53.4 | 0.06 | 1600 | 18 |
| 5 | 40.0 | 0.06 | 10,000 | 20 |

Table 11 Stress and number of cycles for each level in group B5

| Level | S_{\max} (MPa) | R | Number of cycles | f (Hz) |
|-------|------------------|------|------------------|----------|
| 1 | 40.0 | 0.06 | 10,000 | 20 |
| 2 | 53.4 | 0.06 | 1600 | 18 |
| 3 | 130.0 | 0.06 | 27 | 5 |
| 4 | 53.4 | 0.06 | 1600 | 18 |
| 5 | 40.0 | 0.06 | 10,000 | 20 |

Table 12 Stress and number of cycles for each level in group B6

| Level | S_{\max} (MPa) | R | Number of cycles | f (Hz) |
|-------|------------------|------|------------------|----------|
| 1 | 40.0 | 0.06 | 10,000 | 20 |
| 2 | 53.4 | 0.06 | 1600 | 18 |
| 3 | 90.7 | 0.06 | 115 | 5 |
| 4 | 53.4 | 0.06 | 1600 | 18 |
| 5 | 40.0 | 0.06 | 10,000 | 20 |

Table 13 Stress and number of cycles for each level in group B7

| Level | S_{\max} (MPa) | R | Number of cycles | f (Hz) |
|-------|------------------|------|------------------|----------|
| 1 | 40.0 | 0.06 | 10,000 | 20 |
| 2 | 53.4 | 0.06 | 1600 | 18 |
| 3 | 71.0 | 0.06 | 304 | 5 |
| 4 | 53.4 | 0.06 | 1600 | 18 |
| 5 | 40.0 | 0.06 | 10,000 | 20 |

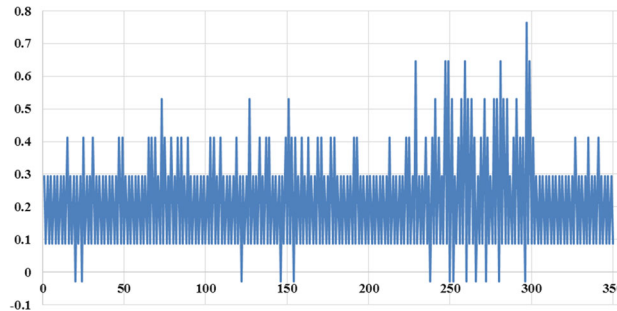
Similarly, stress and strain fields of critical spot near the hole for every cycle in 7 groups of blocked spectrum loading are obtained. The estimated results of fatigue life with post-processor program are listed in Table 15. In addition, S - N curve can be obtained by fitting test results under constant amplitude loading. Then fatigue life predicted by Miner rule [28] are also calculated and listed as comparisons with results obtained by proposed model. It can be seen that maximum error of fatigue life predicted by the proposed model is -21.88% , which is acceptable in engineering. The error of predicted life by Miner rule is larger. This suggests that macro–micro-two-scale damage model takes loading sequential effect into account and the fatigue damage accumulation is nonlinear while Miner rule is only linear accumulation. Besides, all the predicted lives by

Table 14 Test results of 7 groups

| Group | Test life | Mean value of life |
|-------|--|--------------------|
| B1 | 1,63,432, 2,11,870, 1,78,504, 2,66,364, 1,89,127, 3,56,668, 3,31,557, 2,33,564, 3,25,297 | 2,50,709 |
| B2 | 3,79,884, 3,19,442, 3,62,052 | 3,53,793 |
| B3 | 4,60,559, 4,48,434, 2,41,388, 3,34,302 | 3,71,170 |
| B4 | 5,32,729, 6,14,684, 5,67,869, 5,91,359, 5,91,354 | 5,79,599 |
| B5 | 1,716,198, 2,017,294, 2,110,305, 1,911,960, 2,214,947 | 1,994,140 |
| B6 | 1,716,276, 2,091,168, 2,243,471 | 2,016,972 |
| B7 | 2,755,039, 2,255,047, 1,860,186, 1,993,181 | 2,215,863 |

Table 15 Comparisons between test life and predicted life of 7 groups

| Group | Test mean life | Predicted life | Error (%) | Miner predicted life | Miner error (%) |
|-------|----------------|----------------|-----------|----------------------|-----------------|
| B1 | 2,50,709 | 2,09,435 | -16.46 | 1,72,190 | -31.32 |
| B2 | 3,53,793 | 2,78,450 | -21.3 | 1,17,539 | -66.78 |
| B3 | 3,71,170 | 3,70,250 | -0.24 | 1,30,007 | -64.97 |
| B4 | 5,79,599 | 4,76,011 | -17.87 | 2,46,532 | -57.47 |
| B5 | 1,994,140 | 1,557,684 | -21.88 | 3,60,343 | -81.93 |
| B6 | 2,016,977 | 1,743,970 | -16.78 | 3,55,853 | -82.36 |
| B7 | 2,215,863 | 1,744,226 | -21.28 | 3,62,483 | -83.64 |

**Fig. 12** Part of random loading sequence**Table 16** Statistical result of random spectrum loading

| Number | Normalized peak-valley value | Number of peak-valley value | S_{\max} (MPa) |
|--------|------------------------------|-----------------------------|------------------|
| 1 | 1 | 119 | 195.60 |
| 2 | 0.88235 | 360 | 172.58 |
| 3 | 0.765 | 870 | 149.63 |
| 4 | 0.647 | 1995 | 126.55 |
| 5 | 0.529 | 3874 | 103.47 |
| 6 | 0.411 | 7036 | 80.39 |
| 7 | 0.294 | 12,540 | 57.50 |
| 8 | 0.088 | 24,494 | 17.21 |
| 9 | -0.029 | 2180 | -5.67 |
| 10 | -0.147 | 116 | -28.76 |
| 11 | -0.264 | 4 | -51.64 |

Table 17 Test and predicted results under random spectrum loading

| Test life | Mean life | Predicted life | Error (%) | Miner life | Miner error (%) |
|--|-----------|----------------|-----------|------------|-----------------|
| 4,63,603, 4,57,200, 5,04,980, 5,17,070, 3,48,022, 3,65,568 | 4,42,740 | 3,95,692 | -10.63 | 171,646 | -61.23 |

macro–micro–two-scale damage model are shorter than tested mean lives which means the predicted results are conservative.

The random spectrum is a practical loading sequence obtained from a critical component in certain airplane. Part of random loading sequence is illustrated in Fig. 12, and the statistical result of peak-valley stress is listed in Table 16. The test and predicted results are listed in Table 17. It can be seen that the conclusion is consistent with that under blocked spectrum loading.

4.3 Discussions

Although the predicted fatigue life under different loading cases are consonant with test results, it is necessary to note some aspects from the engineering application point of view.

First, the key issue is to identify parameters, such as S , s and q , in macro–micro-two-scale damage model, which requires some basic fatigue test data. So some groups of fatigue test under constant amplitude loading should be performed in advance to identify model parameters for different metal. Second, the proposed model is only used in situation that macroscopic stress is in elastic. Besides, to consider retardation effect properly in random loading sequence, the post-processor calculates microscopic stresses, strains and accumulated damage cycle by cycle, which will increase computational cost.

5 Conclusions

An improved macro–micro-two-scale damage model for metallic material is proposed in the paper. The algorithm framework to compute microscopic elasto-plastic stress–strain along with proposed model is established and coded as post-processor.

Fatigue damage evolution equation at microscale is modified based on Lemaitre damage equation, which accounts for nonlinear plastic hardening, crack closure and mean stress effect. Parameters S , s and q in the equation are fitted using an optimization procedure through 6 groups of constant amplitude fatigue tests under $R = -1$.

To test the validity of the proposed model, 8 groups of constant amplitude tests under different stress ratio have been performed. The maximum error of predicted mean life is -19.02% , which is acceptable in engineering. Besides, tests under 7 groups of blocked spectrum and 1 group of random spectrum loading are added to verify the general applicability of the model. The maximum error is -21.88% . Meanwhile, the error of predicted life by Miner rule is about 3–4 times larger than that by proposed model, which shows the proposed model can quantify loading sequence and mean stress effect under variable amplitude loading.

Acknowledgements This work is supported by the National Natural Science Foundation of China (51375386).

References

- Huang, W., Sridhar, N.: Fatigue failure risk assessment for a maintained Stiffener-Frame welded structure with multiple site cracks. *Int. J. Appl. Mech.* **8**(1), 1650024 (2016)
- Hull, D., Bacon, D.J.: *Introduction to dislocations*. Butterworth-Heinemann, Oxford (2011)
- Gupta, A., Sun, W., Bennett, C.J.: Simulation of fatigue small crack growth in additive manufactured Ti-6Al-4V material. *Continuum Mech. Thermodyn.* (2020). <https://doi.org/10.1007/s00161-020-00878-0>
- Bandara, C.S., Siriwardane, S.C., Dissanayake, U.L., et al.: Developing a full range S-N curve and estimating cumulative fatigue damage of steel elements. *Comput. Mater. Sci.* **96**, 96–101 (2015)
- Todinov, M.T.: Necessary and sufficient condition for additivity in the sense of Palmgren-Miner rule. *Comput. Mater. Sci.* **21**, 101–110 (2001)
- Vasudevan, A.K., Sadananda, K., Iyyer, N.: Fatigue damage analysis: issues and challenges. *Int. J. Fatigue* **82**, 120–133 (2016)
- Lemaitre, J., Desmorat, R.: *Engineering Damage Mechanics*. Springer, Berlin (2005)
- Elshelby, J.D.: The determination of the elastic field of an ellipsoidal inclusion and related problems. *Proc. R. Soc. Lond.* **A241**, 376–396 (1957)
- Hill, R.: Continuum micro-mechanics of elastoplastic polycrystals. *J. Mech. Phys. Solids* **13**, 89–101 (1965)
- Hill, R.: On constitutive macro-variables for heterogeneous solids at finite strain. *Proc. R. Soc. Lond.* **A241**, 131–147 (1972)
- Iwakuma, T., Nemat-Nasser, S.: Finite elastic-plastic deformation of poly-crystalline metals. *Proc. R. Soc. Lond.* **A394**, 87–119 (1984)
- Kröner, E.: On the plastic deformation of polycrystals. *Acta Metallurgica* **9**, 155–161 (1961)
- Berveiller, M., Zaoui, A.: Self-consistent schemes for heterogeneous solid mechanics. In *Comportement Rhéologique et Structure des Matériaux*, CR 15è coll. GFR, Paris (1980)
- Pierard, O., Gonzalez, C., Segurado, J., et al.: Micromechanics of elasto-plastic materials reinforced with ellipsoidal inclusions. *Int. J. Solids Struct.* **44**, 6945–6962 (2007)
- Lemaitre, J.: *A Course on Damage Mechanics*. Springer, Berlin (1992)
- Lemaitre, J., Desmorat, R., Sauzay, M.: Anisotropic damage law of evolution. *J. Mech. Theor. Appl.* **19**, 187–208 (2000)
- Lemaitre, J., Doghri, I.: Damage 90: a post processor for crack initiation. *Comput. Method Appl. Mech. Eng.* **115**, 197–232 (1994)
- Lemaitre, J., Sermage, J.P., Desmorat, R.: A two scale damage concept applied to fatigue. *Int. J. Fract.* **97**, 67–81 (1999)
- Laiarinandrasana, L., Morgener, T.F., Cheng, Y., et al.: Microstructural observations supporting thermography measurements for short glass fibre thermoplastic composites under fatigue loading. *Continuum Mech. Thermodyn.* **32**, 451–469 (2020). <https://doi.org/10.1007/s00161-019-00748-4>
- Sun, B., Xu, Y.L., Li, Z.: Multi-scale fatigue model and image-based simulation of collective short cracks evolution process. *Comput. Mater. Sci.* **117**, 24–32 (2016)

21. Lautrou, N., Thevenet, D., Cognard, J.Y.: Fatigue crack initiation life estimation in a steel welded joint by the use of a two-scale damage model. *Fatigue Fract. Eng. Mater. Struct.* **32**(5), 403–417 (2009)
22. Qian, C., Westphal, T., Nijssen, R.P.L.: Micro-mechanical fatigue modelling of unidirectional glass fibre reinforced polymer composites. *Comput. Mater. Sci.* **69**(1), 62–72 (2013)
23. Lemaitre, J., Sermage, J.P.: One damage law for different mechanisms. *Comput. Mech.* **20**, 84–88 (1997)
24. Eggertsen, P., Mattiasson, K.: On the identification of kinematic hardening material parameters for accurate springback predictions. *Int. J. Mater Form* **4**, 103–120 (2011)
25. Bathe, K.J., Montans, F.J.: On modeling mixed hardening in computational plasticity. *Comput. Strut.* **82**(6), 535–539 (2004)
26. Nijssen, R.P.L., Van Delft, D.R.V., Van Wingerde, A.M.: Alternative fatigue lifetime prediction formulations for variable-amplitude loading. *J. Sol. Energy Eng.* **124**(4), 396–403 (2002)
27. Burger, M., Wolfram, M.: Numerical approximation of an SQP-type method for parameter identification. *SIAM J. Numer. Anal.* **40**, 1775–1797 (2002)
28. Miner, M.A.: Cumulative damage in fatigue. *J. Appl. Mech.* **14**, A159–164 (1945)

Publisher's Note Springer Nature remains neutral with regard to jurisdictional claims in published maps and institutional affiliations.